Inorganic Chemistry

pubs.acs.org/IC Article

Heteronuclear Iron(III)−Schiff Base Complexes with the Hexacyanidocobaltate(III) Anion: On the Quest To Understand the Governing Factors of Spin Crossover

Ján Pavlik, Petra Masárová, Ivan Nemec, Olaf Fuhr, Mario Ruben, and Ivan Šalitroš*

Cite This: https://dx.doi.org/10.1021/acs.inorgchem.9b03097 Read Online

ABSTRACT: Two heteronuclear compounds (**1** and **2**) containing three ferric centers linked in facial-like mode with the magnetically silent hexacyanidocobaltate(III) anion were prepared and studied. The structural investigation revealed that both compounds are tetranuclear complexes with molecular formulas of $[\{Fe(L1)NC\}_3Co(CN)_3]\cdot 2CH_3OH\cdot 2.5CH_3CN$ (**1**) and $[\{Fe(L2)NC\}_3Co(CN)_3]\cdot 2H_2O\cdot 1CH_3OH$ (**2**). The magnetic properties of both complexes are controlled by the molecular design of the corresponding pentadentate Schiff base anions $L1^{2-}$ and $L2^{2-}$. While compound **2** with a symmetric ligand prepared from salicylaldehyde shows high-spin state properties, compound **1** containing the asymmetric ligand with naphthalene units either is low-spin in its solvated form or shows a gradual but hysteretic spin crossover event when desolvated. The magnetic behavior was analyzed with respect to the Ising-like model and spin Hamiltonian, respectively, and the results were confronted with *ab initio* calculations. Additionally, the influence of structural features, lattice solvent molecules, the distribution of electronic terms, and active orbitals on the spin state properties of reported complexes is discussed.

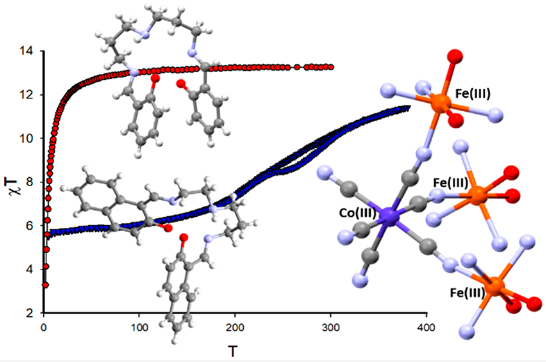

INTRODUCTION

Fe(III)−Schiff base (SB) complexes present one of the most explored families of spin crossover (SCO) compounds.[1] The simplicity of SB condensation allows the usually undemanding preparation of chelating N- or N,O-donor ligands with various substituents capable of controlling the intermolecular cooperativity of corresponding complexes as well as the transition temperature of their SCO. Thus, the rationalized molecular design of the polydentate SB ligands is the pivotal step in the synthesis of the complexes exhibiting an abrupt and room-temperature hysteretic transition of spin.[2]

The formation of mononuclear ferric complexes with chelating tetradentate [i.e., salen = *N*,*N*′-bis(salicylidene)-ethylenediamine] or pentadentate [i.e., saldien = *N*,*N*′-bis(salicylidene)diethylenetriamine] SB ligands and their further interconnection with N-donor bridging ligands usually result in coordination polymers with one-dimensional (1D),[3] two-dimensional (2D),[4] or three-dimensional (3D)[5] supramolecular architecture or low-dimensional discrete polynuclear compounds.[6] Fe(III) central atoms are then surrounded with a N_4O_2-donor atom set that supports the occurrence of SCO. Taking advantage of the ambidentate character of cyanido ligands in $[M(CN)_6]^{y-}$ types of anions (where M is a first-row transition metal), one finds that the hexacyanidometalates serve as excellent bridging ligands, as well. For instance, the [Fe(L)Cl] type of complex (where L is a pentadentate N_3O_2-donor derivative of saldien) in combination with the ferrocyanide anion forms heptanuclear mixed-valence compounds in which all six cyanido ligands connect {Fe(L)} moieties. In this case, ferric centers are surrounded with N_4O_2-donor atoms and therefore either show thermally induced SCO[7] or permanently persist in a high-spin (HS) state.[8] Also, trivalent anions $[M(CN)_6]^{3-}$ [where M = Fe(III), Mn(III), Cr(III), or Co(III)] can play the role of hexadentate bridging ligands.[8a,9] However, only a handful of polynuclear compounds containing ferric complex moieties were coordinated on the $[M(CN)_6]^{3-}$ backbone in which some of the cyanide anions have a bridging character and the rest act as terminal ligands.[10] For instance, Gao and Sato reported a trinuclear complex in which the $[Cr(CN)_6]^{3-}$ anion coordinates two HS ferrous complex units and shows slow relaxation of AC susceptibility at zero static magnetic field.[10a] On the other hand, gradual and room-temperature SCO was studied in pentanuclear systems with hexacyanidoferrate(III) or hexacyanidocobaltate(III) cores capable of interconnecting three Fe(II)−phenanthroline centers.[10b] Herchel and co-workers introduced {Fe(L)} ferric

Received: October 24, 2019

Scheme 1. Molecular Structures of Pentadentate Schiff Bases H_2L1 and H_2L2 (left) and Schematic Preparation of Tetranuclear Complexes 1 and 2 (right)

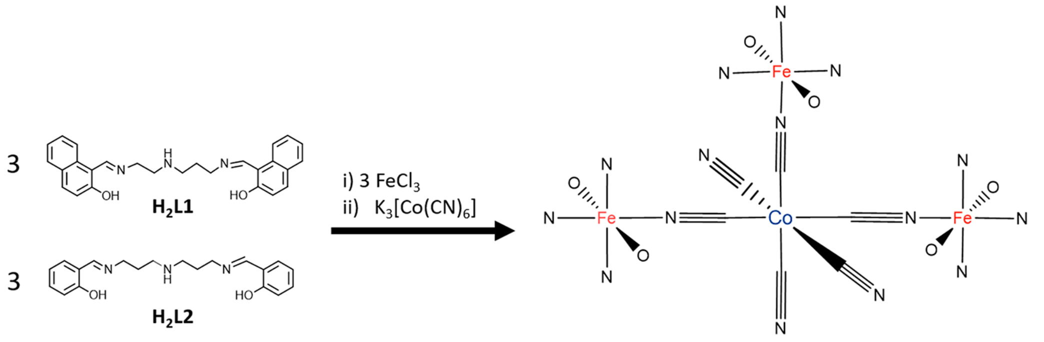

Compound 1: $[\{Fe(L1)NC\}_3Co(CN)_3]\cdot 2CH_3OH\cdot 2.5CH_3CN$
Compound 2: $[\{Fe(L2)NC\}_3Co(CN)_3]\cdot CH_3OH\cdot 2H_2O$

moieties onto the hexacyanidochromate(III) complex anion, which resulted in the formation of a tetranuclear T-shaped {Fe(III)$_3$-Cr(III)} complex with a meridional-like arrangement of Fe(III) centers. A detailed magnetic study allowed the investigation of the interesting interplay between gradual thermal SCO of ferric centers and exchange coupling mediated through the paramagnetic central atom of the $[Cr(CN)_6]^{3-}$ bridging anion.[10c] The nature of the Fe(III)−Cr(III) magnetic exchange coupling strongly depends on the spin state of the SCO active ferric centers and changes between antiferromagnetic in their HS and ferromagnetic in their low-spin (LS) states.

Inspired by the idea of polynuclear SCO complexes whose molecular structure contains hexacyanidometalate anions, we prepared and investigated similar compounds with magnetically silent hexacyanidocobaltate(III) bridges to prevent the magnetic exchange interactions between Fe(III) SCO centers. Two tetranuclear complexes (**1** and **2**) were synthesized from mononuclear ferric precursors [Fe(L1)Cl] and [Fe(L2)Cl], respectively, containing the different pentadentate ligand dianions (doubly deprotonated SBs H_2L1 = 1-((*Z*)-((3-((2-((*E*)-((2-hydroxynaphthalen-1-yl)methylene)amino)ethyl)-amino)propyl)imino)methyl)naphthalen-2-ol and H_2L2 = 2,2′-((1*E*,1′*E*)-((azanediylbis(propane-3,1-diyl))bis-(azanylylidene))-bis(methanylylidene))-diphenol, respectively) (Scheme 1). Their magnetic behavior varies with the structural differences of the used SB ligands. While complex **1** with a SB ligand prepared from the asymmetric triamine and 2-hydroxynaphthaldehyde (Scheme 1) shows solvent-dependent SCO properties, complex **2** containing the SB ligand with symmetric *N*,*N*-bis(propylene)amino aliphatic and phenylene aromatic parts shows permanent HS properties. The magnetic properties of both compounds were analyzed using empirical models and state-of-the-art quantum chemistry calculations and discussed in a comparative manner to identify the key factor of their different SCO behavior.

Table 1. Crystallographic Data for Compounds 1 and 2

	1 ($[\{Fe(L1)NC\}_3Co(CN)_3]\cdot 2CH_3OH\cdot 2.5CH_3CN$)	**2** ($[\{Fe(L2)NC\}_3Co(CN)_3]\cdot CH_3OH\cdot 2H_2O$)
formula	$C_{94}H_{90.50}CoFe_3N_{17.50}O_8$	$C_{67}H_{77}CoFe_3N_{15}O_9$
formula weight (g mol^{-1})	1819.81	1462.92
crystal color	black	black
temperature (K)	180(2)	150(2)
wavelength (Å)	0.71073	0.71073
crystal system	triclinic	orthorhombic
space group	$P\bar{1}$	*Pbca*
a (Å)	14.275(3)	13.4046(6)
b (Å)	16.462(3)	26.5848(9)
c (Å)	19.515(4)	38.3752(12)
α (deg)	80.90(3)	90
β (deg)	87.95(3)	90
γ (deg)	80.73(3)	90
V (Å^3)	4468.8(16)	13675.3(9)
Z, ρ_{calc} (g cm^{-3})	2, 1.352	8, 1.421
μ (Mo Kα) (mm^{-1})	0.726	0.929
F(000)	1892	6088
crystal size (mm)	0.32 × 0.29 × 0.24	0.28 × 0.24 × 0.22
θ range for data collection (deg)	1.057−23.736	2.947−25.227
no. of reflections collected	22783	72038
no. of independent reflections	12728 (R_{int} = 0.0752)	12019 (R_{int} = 0.1619)
no. of independent reflections with $I \geq 2\sigma(I)$	7217	5962
data/restraints/parameters	12728/8/1112	12019/3/864
final *R* indices [$I \geq 2\sigma(I)$]	R_1 = 0.0723, wR_2 = 0.1856	R_1 = 0.0596, wR_2 = 0.1642
R indices (all data)	R_1 = 0.1323, wR_2 = 0.2104	R_1 = 0.1214, wR_2 = 0.1769
goodness of fit on F^2	0.998	0.888
CCDC deposit number	1869404	1954726

■ STRUCTURAL INVESTIGATION

The synthesis and characterization of tetranuclear complexes **1** and **2** are described in the Experimental Section. Compound **1** crystallizes in triclinic space group $P\bar{1}$, and its molecular formula as well as its asymmetric unit in the crystal structure can be expressed as $[\{Fe(L1)NC\}_3Co(CN)_3]\cdot 2CH_3OH\cdot 2.5CH_3CN$ (select crystallographic information is listed in Table 1). The tetranuclear complex contains the hexacyanidocobaltate(III) core on which three {Fe(L1)} ferric units are coordinated via N-donor atoms of cyanido bridging ligands adopting a facial-like arrangement (Figure 1a). Fe(III) coordination centers are surrounded by five N_3O_2-donor atoms of the SB ligand anion with a *cis*-O_2/*mer*-N_3 configuration. The sixth cyanido N-donor atom (denoted as N_{CN}) is in an axial position with respect to one of two O-donor atoms (O_{ax}), while the second oxygen (O_{eq}) together with two imino

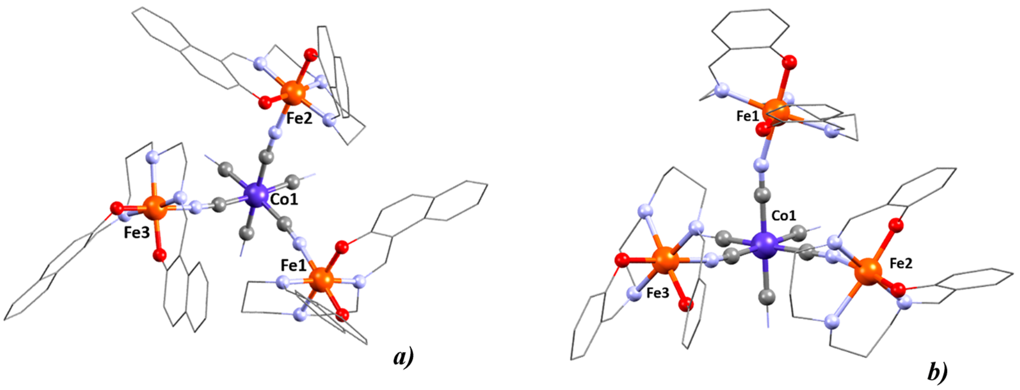

Figure 1. Molecular structure of complexes (a) **1** and (b) **2**. Hydrogen atoms and lattice solvent molecules have been omitted for the sake of clarity. Color code: C, gray; N, light blue; O, red; Fe, orange; Co, dark blue.

Table 2. Selected Bond Distances and Structural Parameters of Compounds 1 and 2[a]

	1			2		
	Fe1	Fe2	Fe3	Fe1	Fe2	Fe3
$\mathrm{Fe{-}N_{im}}$ (Å)	1.949(6)	1.934(7)	1.903(6)	2.106(5)	2.079(6)	2.100(5)
$\mathrm{Fe{-}N_{im}}$ (Å)	1.914(6)	1.907(9)	1.957(6)	2.124(5)	2.123(6)	2.119(6)
$\mathrm{Fe{-}N_{am}}$ (Å)	2.017(6)	2.003(6)	2.000(6)	2.196(5)	2.208(5)	2.188(5)
$\mathrm{Fe{-}N_{CN}}$ (Å)	1.966(7)	1.958(7)	1.949(6)	2.097(6)	2.075(5)	2.093(6)
$\mathrm{Fe{-}O_{eq}}$ (Å)[b]	1.866(6)	1.888(5)	1.874(5)	1.933(4)	1.940(4)	1.957(4)
$\mathrm{Fe{-}O_{ax}}$ (Å)[b]	1.871(6)	1.882(5)	1.876(4)	1.941(4)	1.929(4)	1.917(4)
Σ (deg)	20.2	19.7	26.4	36.8	37.1	25.7
Θ (deg)	33.8	36.6	53.7	95.8	88.5	56.0
S(OC-6)	0.12	0.11	0.19	0.47	0.40	0.27
S(TPR-6)	15.90	15.92	15.28	14.04	14.44	15.53

[a] $\mathrm{Fe{-}N_{im}}$, $\mathrm{Fe{-}N_{am}}$, and $\mathrm{Fe{-}N_{ps}}$ represent distances for bonds between the iron(III) central atom and the corresponding imino ($\mathrm{N_{im}}$), amino ($\mathrm{N_{am}}$), and pseudohalide ($\mathrm{N_{ps}}$) nitrogen-donor atoms. [b] $\mathrm{O_{eq}}$ and $\mathrm{O_{ax}}$ are O-donor atoms in the equatorial and axial positions, respectively, with respect to the N-donor atom of the cyanido ligand.

nitrogen atoms ($\mathrm{N_{im}}$) and one amino nitrogen atom ($\mathrm{N_{am}}$) is placed in the equatorial plane. Pentadentate SB ligands can form a wreath around the metal centers in a clockwise (Δ) or anticlockwise (Λ) manner (Figure S2). All {Fe(L1)} moieties of two complex molecules involved in the centrosymmetric unit cell contain both helical orientations; however, chelating ligands in {Fe1(L1)} and {Fe2(L1)} adopt the opposite orientation compared to the third center, {Fe3(L1)}. The shortest bonds of coordination polyhedra are formed with oxygen-donor atoms (d_{avg} = 1.88 Å), and average values of $\mathrm{Fe{-}N_{im}}$, $\mathrm{Fe{-}N_{CN}}$, and $\mathrm{Fe{-}N_{am}}$ bond distances at 180 K (1.93, 1.96, and 2.01 Å, respectively) are typical for the LS state of Fe(III) coordination centers (Table 2).[11] Angular distortion parameters Σ and Θ are good indicators of the spin state in a given metal center. In agreement with a previously published structural investigation of similar Fe(III) SCO complexes with a $\mathrm{N_4O_2}$ coordination environment (Figure S1),[12] their calculated values (Σ ≈ 20°; Θ ≈ 33–56°) are typical for the LS state and along with symmetry measurement parameters proposed by Alvarez et al. [*S*(OC-6) ≈ 0.1 (Table S1)][13] suggest only weak deviation from octahedral symmetry in all four metal centers of **1**. The Co(III) center is surrounded by six C-donor atoms of cyanido bridging ligands, and Co–C bond distances vary in the narrow range of 1.88–1.90 Å, suggesting the LS state of the metal center (Table S2).

Compound **2** crystallizes in orthorhombic space group *Pbca* (Table 1), and its asymmetric unit is identical with the molecular formula expressed as $[\{\mathrm{Fe(L2)NC}\}_3\mathrm{Co(CN)_3}]\cdot\mathrm{CH_3OH}\cdot 2\mathrm{H_2O}$ (Figure 1b). Also in this case, three {Fe(L2)} moieties are facially coordinated on the $[\mathrm{Co(CN)_6}]^{3-}$ anion forming the neutral tetranuclear complex. All three ferric centers are surrounded by four N-donor atoms (two imino $\mathrm{N_{im}}$, one amino $\mathrm{N_{am}}$, and one cyanido $\mathrm{N_{CN}}$) and two O-donor atoms ($\mathrm{O_{ax}}$ axial with respect to $\mathrm{N_{CN}}$ and equatorial $\mathrm{O_{eq}}$). One SB ligand coordinates one Fe(III) center with all five donor atoms adopting the *cis*-$\mathrm{O_2}$/*mer*-$\mathrm{N_3}$ configuration. Contrary to complex **1**, the formation of a wreath of pentadentate ligand anion $\mathrm{L2^{2-}}$ is the same in all three {Fe(L2)} moieties of one molecule and the centrosymmetric unit cell contains four tetranuclear molecules with the Λ and another four with the Δ helical orientation. Fe–N bond distances [$d_{\mathrm{avg}}(\mathrm{Fe{-}N_{im}})$ = 2.11 Å, $d_{\mathrm{avg}}(\mathrm{Fe{-}N_{CN}})$ = 2.09 Å, and $d_{\mathrm{avg}}(\mathrm{Fe{-}N_{am}})$ = 2.20 Å] indicate the HS state at 150 K. Also, angular distortion parameters exhibit values typical for the HS Fe(III) complexes [Σ ≈ 33°; Θ ≈ 80° (Table 2)] and along with the symmetry measure parameters [*S*(OC-6) ≈ 0.4 (Table S1)] indicate a slightly elevated degree of distortion of three Fe(III) centers compared to those found in **1**.[11]

In the crystal structures of both reported compounds, the tetranuclear complex molecules are not directly interconnected by mutual hydrogen bonding, but the present lattice solvent molecules mediate formation of hydrogen bonding networks. During X-ray diffraction measurements, we observed that the crystal quality of both compounds is significantly affected by the solvent loss, which resulted in problematic modeling of the

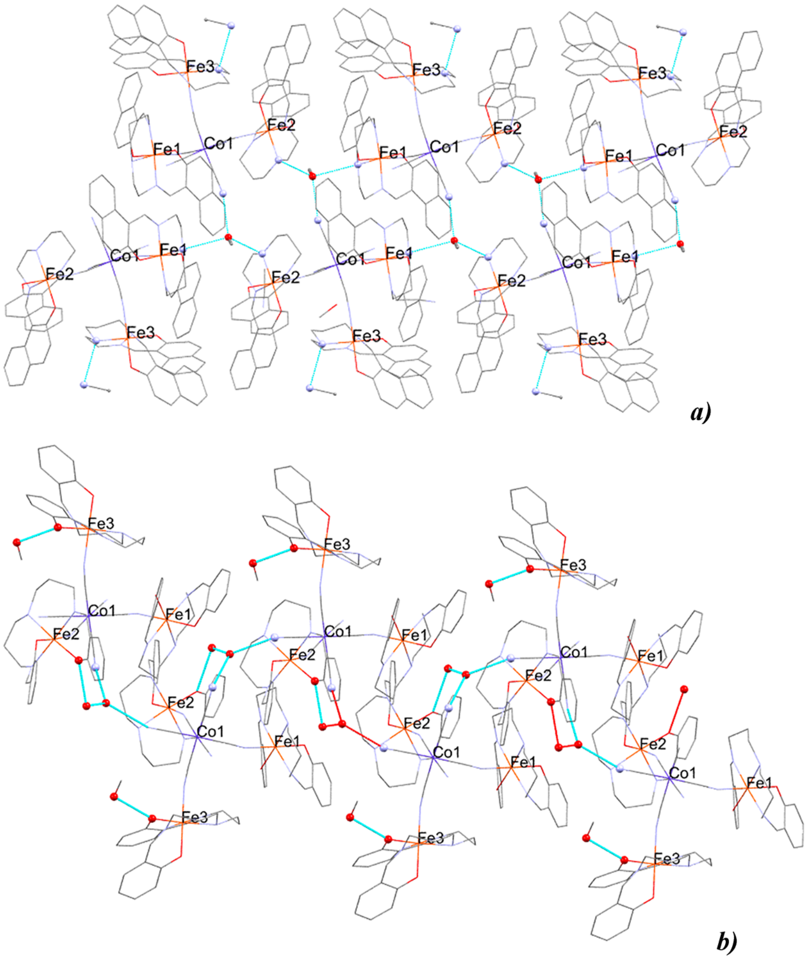

Figure 2. Hydrogen bonding network in the crystal structures of compounds (a) **1** and (b) **2**. Hydrogen atoms have been omitted for the sake of clarity. Color code: C, gray; N, light blue; O, red; Fe, orange; Co, dark blue. Cyan dashed lines represent H-bonds.

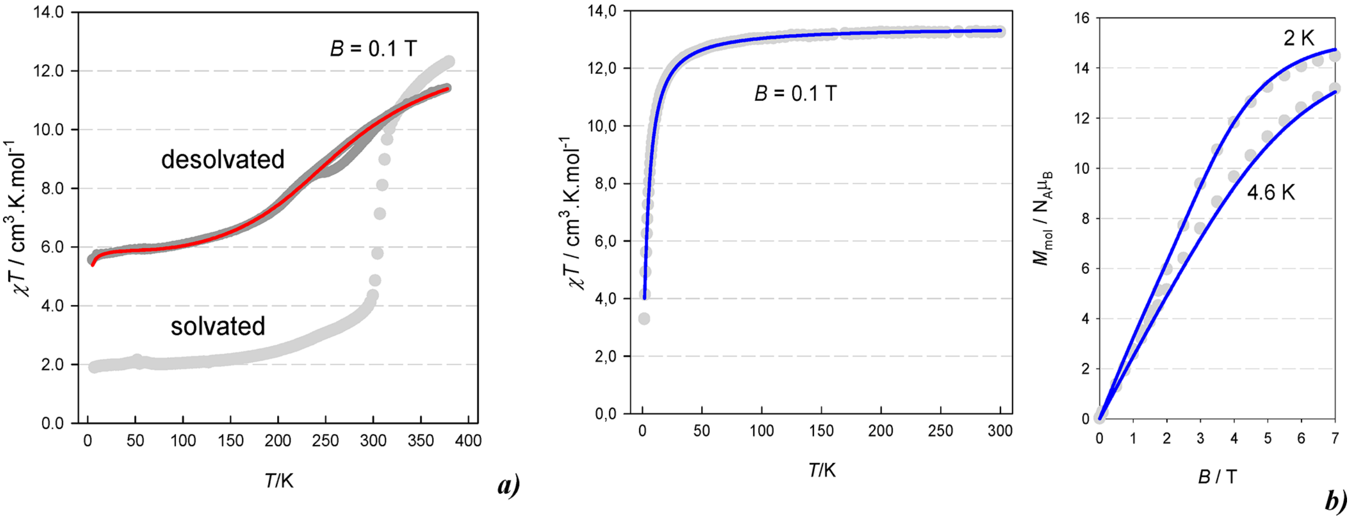

Figure 3. (a) Temperature dependence of the χT product for solvated (pale gray points) and desolvated **1** (dark gray points, experiment; red solid line, optimum fit). (b) Optimum fit of isothermal variable field magnetization curves of compound **2** using model 2 (points, experiment; solid line, optimum fit).

solvent molecules and nonroutine aspects of structural refinement (for details, see the Experimental Section).

In the case of **1**, one molecule of methanol interconnects three neighboring complex molecules via one O−H···N and two N−H···O hydrogen bonds (HBs). The oxygen atom of the methanol molecule acts as an acceptor in two HBs formed with the amino groups of two nonidentical {Fe(L1)} entities [d(N···O) = 3.102(9) and 2.954(9) Å], whereas it acts as a donor in a HB with the nitrogen atom from one of the monodentate coordinated cyanido ligands [d(O···N) =

https://dx.doi.org/10.1021/acs.inorgchem.9b03097
Inorg. Chem. XXXX, XXX, XXX−XXX

2.728(9) Å]. In this manner, the 2D supramolecular network along the *a*−*b* plane is formed (Figure 2a). Two other methanol molecules and the phenolic oxygen atom of the {Fe(L1)} moiety are linked together in the supramolecular chain by two O−H···O HBs, and the donor−acceptor distance is slightly shorter for the contact found between the methanol molecules [*d*(O···O) = 2.855(9) vs 2.734(9) Å]. One of the acetonitrile molecules forms a N−H···N HB with the amine group of the {Fe(L1)} moiety, while the other two are involved in weak C−H···N noncovalent interactions.

In **2**, two water molecules mediate the formation of a 1D supramolecular zigzag chain along the *a* axis (Figure 2b) via four O−H···A HBs (A = N or O). Two O−H···N HBs are formed between the water molecules and the monodentately coordinated cyanido ligands of the adjacent tetranuclear complexes [*d*(O···N) = 2.908(4) and 2.910(4) Å]. In the case of O−H···O HBs, the donor···acceptor distance is slightly shorter for the HB formed between two water molecules [*d*(O···O) = 2.809(4) Å] than one found between the water molecule and the phenolic oxygen atom of the {Fe(L2)} moiety [*d*(O···O) = 2.908(4) Å]. The methanol molecule in the crystal structure of **2** is not involved in the formation of the supramolecular chain, but it also forms an O−H···O HB with the phenolic oxygen atom of the {Fe(L2)} moiety [*d*(O···O) = 2.809(4) Å]. It must be noted that the crystal structure of **2** also contains other lattice solvent molecules, and these form a chain of O−H···O HBs interconnecting the water and methanol molecules mentioned above. However, they exhibit positional disorder (H_2O···H_2O vs CH_3OH), and furthermore, the methanol molecule is disordered over two positions. Hence, it was not possible to model this part of the crystal structure reasonably.

■ MAGNETIC PROPERTIES AND COMPUTATIONAL STUDY

The magnetism of **1** and **2** shows considerable differences (Figure 3). Complex **1** in its solvated form exhibits a magnetic response typical for LS Fe(III) systems up to 300 K (Figure 3a, pale gray points). Above this temperature, the lattice solvent release takes a place as indicated by TG-DTA (Figure S3), which causes irreversible transformation from the solvated LS to desolvated SCO active form. Further temperature sweeping of desolvated system **1** revealed the presence of gradual and incomplete SCO accompanied by a thermal hysteresis of an unusual shape, which is stable within two consecutive cooling/heating cycles (Figure S4a). As the ratio of the frozen HS state is very close to one-third, we can speculate that one of three Fe centers in the molecule maintains its spin state. In such a case, the SCO event of **1** can be schematically written as HHH ↔ HLL. In contrast, temperature-dependent magnetic measurement of **2** in its solvated form indicates HS state behavior that is not affected by the lattice solvent release at 400 K (Figures S3b and S4b).

The spin crossover in the desolvated form of **1** was analyzed using the most popular form of the Ising-like model.[14] The transition curve is described by the implicit equation

$$x = \frac{r_{\mathrm{eff}}}{r_{\mathrm{eff}} + \exp[\beta(\Delta_{\mathrm{eff}} + \gamma - 2\gamma x)]} \qquad (1)$$

where $\beta = 1/(k_B T)$, Δ_{eff} is the effective energy difference between HS and LS states, γ is the cooperativity, and r_{eff} is the temperature-dependent effective degeneracy ratio between the HS and LS forms. This quantity is related to the mean vibrational frequency ($\bar{\nu}$) of the chromophore in the HS state as[15]

$$r_{\mathrm{eff}} = \left\{ \frac{1 - \exp[-1.5\beta h\bar{\nu}(\mathrm{HS})]}{1 - \exp[-\beta h\bar{\nu}(\mathrm{HS})]} \right\}^{15} \qquad (2)$$

In this approximation, electronic degeneracy can be omitted because the higher spin multiplicity of the HS state is compensated by the higher orbital degeneracy of the LS state. To determine the incompleteness of the SCO event, a renormalization was introduced as

$$x_{\mathrm{renorm}} = x_{\mathrm{frz}} + (1 - x_{\mathrm{frz}})x \qquad (3)$$

The HS state of **1** at high temperatures can be approximated well by the Curie−Weiss law with a fixed *g* factor equal to 2.000.[16] The magnetism of the LS state is expected to be more complex; nevertheless, for the sake of simplicity, it was treated as a Curie paramagnet, too. The Weiss constant was introduced only for the HS state and presented in its microscopic form as a molecular field correction with parameter *zJ*. The best fit of the SCO curve of **1** is displayed in Figure 3a, and optimum values of model parameters are listed in Table 3. The tight hysteresis loop was not identified within this simplistic model.

Table 3. Summary of Fitted Magnetic Parameters of the Desolvated Form of 1

g(LS)	zJ(HS) (cm^{-1})	x_{frz}	Δ_{eff} (K)	γ (K)	$\bar{\nu}$	R
2.138	−0.615	0.393	201	105	530	1.8

The hypothesis of a specific center keeping its HS state was tested using a density functional theory (DFT) calculation. A model system was defined as being comprised of the molecule itself and two methanol molecules ($[\{Fe(L1)NC\}_3Co(CN)_3]\cdot 2CH_3OH$) found by a low-temperature X-ray study inside the complex cavity. Although the presence of solvent molecules after the desolvation process is questionable, their presence was vital for the model as they prevent collapse of the whole molecular structure. The HLL state was defined by setting the total spin multiplicity equal to 8, and its geometry was optimized by employing the functional TPSS that shows favorable performance for assessment of the ground spin state in transition metal complexes.[17] In other words, the model was left free to assign the center with a stronger tendency for the HS state. As a reference, the same calculation was performed for the HHH state defined by a total spin multiplicity of 16. In the second step, the resulting geometry was refined with a hybrid form of the previous functional, i.e., TPSSh, and a higher-quality basis for iron centers (see the computational details in the Experimental Section). The calculated value of Δ_{eff}(DFT) is 7522 K (Table S3). Despite its correct sign, it is one order of magnitude higher than the value extracted from the fitting of experimental data to the Ising-like model (Table 3). The high-temperature limit of the degeneracy ratio is found to be equal to $\lim_{T\to\infty} r_{\mathrm{eff}}(\mathrm{DFT}) = 145$, thus meeting the order of magnitude of the high-temperature value expected by the fitting model, i.e., $1.5^{15} \approx 438$. As a result, the center Fe2, which is connected with the methanol molecule by hydrogen bonding (Figure 4 and Table S4), was identified as the one that preserves its HS state. Nevertheless, as not much is known

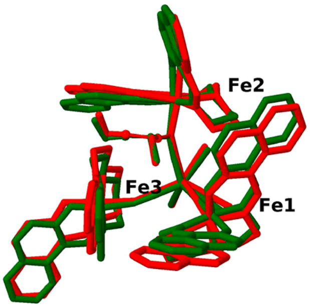

Figure 4. Comparison of the optimum geometries of the HHH state (red) and HLL state (green) in partially solvated **1** ([{Fe(L1)-NC}$_3$Co(CN)$_3$]·2CH$_3$OH). Hydrogen atoms have been omitted for the sake of clarity, except of those in methanol molecules that are part of the H-bond.

about the molecular surroundings after desolvation, such a conclusion has to be made very cautiously, and the alternative with statistically distributed HS centers cannot be dismissed.

Magnetic functions of **2** (Figure 3b) approach the limit of three non-interacting octahedrally coordinated HS Fe(III) centers, for which the low-field high-temperature value of the χT product saturates at 13.1 cm^3 K mol^{-1} and the high-field low-temperature magnetization at 15.00$N_A\mu_B$. To describe its magnetic behavior, three models were tested. In model 1, the spin Hamiltonian is postulated as follows

$$\hat{H} = D \sum_{i=1,2,3} \hat{S}_{iz}^{\ 2} + \mu_B B g_{avg} \sum_{i=1,2,3} \hat{\mathbf{I}}_i \hat{\mathbf{S}}_i - zJ \sum_{i=1,2,3} \langle S_{iz} \rangle \hat{S}_{iz} \tag{4}$$

where D is the axial component of the zero-field splitting, g_{avg} is the average value of the g factor, $\hat{\mathbf{I}}_i$ is the unitary vector operator of the ith center, zJ is the parameter of the molecular field (microscopic representation of the Weiss constant), and μ_B is the Bohr magneton. The index runs over all centers in the molecule (1 for Fe1, etc.). In model 2, the intramolecular exchange interaction was accounted for by adding the following term to the Hamiltonian (eq 4)

$$\hat{H}_{ex} = -J\hat{S}_1\hat{S}_2 - J\hat{S}_2\hat{S}_3 - J\hat{S}_3\hat{S}_1 \tag{5}$$

Finally, model 3 differs from model 2 in the neglect of the effect of the molecular field to test its interplay with intermolecular magnetic exchange interaction. The optimum parameters and residuals for all three models are listed in Table 4. One can conclude that the best agreement with experiment was obtained using model 2 (solid lines, Figure 3b). Although model 1 can satisfactorily describe the temperature function of the susceptibility product, too, it fails when both experimental data sets are confronted (Table 4 and Figure S5a). Despite the fact that the molecular field correction in model 1 has almost the same value as the magnetic exchange parameter in model 2, it is not capable to grasp the shape of the magnetization function. On the other hand, purely intramolecular interaction as considered in model 3 provides a worse fit than model 2 (Table 4 and Figure S5b). Therefore, the presence of dominant intramolecular magnetic exchange interaction and very weak intermolecular interaction can be identified in **2**. On the basis of all of the models used, the presence of magnetic anisotropy is inconclusive; although if it is present, models 2 and 3 suggest its vanishing value in accordance with expectation.[16]

Table 4. Summary of Fitted Magnetic Parameters of System 2 Using Various Models

model	J (cm^{-1})	D (cm^{-1})	g_{avg}	zJ (cm^{-1})	R
model 1	–	0(5)	2.033(5)	−0.231(8)	49.4
model 2	−0.230(3)	0.0(2)	2.036(4)	0.015(2)	8.3
model 3	−0.227(5)	0.0(5)	2.053(7)	–	26.0

The optimum fit values of magnetic parameters have been confronted with the state averaged complete active space self-consistent field calculation combined with N-electron valence perturbation theory of second order (SA-CASSCF+NEVPT2) for all six individual centers {Fe(L1)NC} and {Fe(L2)NC} (parameters D and g) and DFT calculation with the functional B3LYP (parameter J for **2**). Two complete active spaces (CASs) were tested; the first one was constructed with five electrons in five orbitals (3 × t_{2g} + 2 × e_g*), while the second one with nine electrons in 12 orbitals (2 × e_g + 3 × t_{2g} + 2 × e_g* + 5 × 4d). The geometry of the centers and the molecule was kept as provided by X-ray analysis. As observed also in previous studies,[18] only the model with an extended active space reproduced correctly the ground spin state for the experimental geometry of individual centers, i.e., doublet for centers of **1** and sextet for centers of **2** (Figure 5). This is in agreement with the results of the structural and magnetic study of LS compound **1** in its solvated form and HS compound **2**. The HS state for Fe2 in partially solvated molecule **1** ([{Fe(L1)NC}$_3$Co(CN)$_3$]·2CH$_3$OH) as assessed by DFT (*vide supra*) was not confirmed by this more reliable approach. This, however, does not contradict the experimental results because in the fully solvated form of **1** ([{Fe(L1)NC}$_3$Co(CN)$_3$]·2CH$_3$OH·2.5CH$_3$CN) the complete LS state was observed. The values resulting from the extended CAS are listed in Table 5 (for results from smaller CASs and other details, see Tables S5 and S6).

As is apparent, the calculated g factors are overestimated for the LS state of **1** and underestimated with respect to any model of fitting for **2**. The calculated values of the axial magnetic anisotropy of **2** span the limit typical in this class of compounds.[11] In **1**, the anisotropy parameters are not defined as it possesses an LS state (S = $^1/_2$). Because the rhombicity factor E/D approaches $^1/_3$ for the center Fe3 of **2**, the sign of its axial magnetic parameter is arbitrary. Absolute values of magnetic exchange parameters estimated by DFT are 1 order of magnitude lower than the fitted values. Moreover, they do not agree with each other in sign, which is probably caused by approaching the numerical limits of the method, i.e., diminishing energy changes calculated for a huge system.

Although the energy of vertical excitations cannot be identified with the SCO energy difference Δ_{eff} because the molecular geometry changes during the genuine SCO, the contrast in the accessibility of excited spin states between centers of complexes **1** and **2** is remarkable (Figure 5). To understand this effect more deeply, the active orbitals from the extended CAS were inspected. The only noticeable difference between **1** and **2** was found in their bonding e_g orbitals. In complex **2**, one of these orbitals is considerably delocalized to the π-system of the neighboring aromatic ring and has a lower occupancy number. In contrast, the corresponding e_g orbital in **1** is localized well on the Fe(III) coordination chromophore (Figure 6 and Figure S6). For the comparison, the same computational approach was applied on the previously reported compound [{Fe(L2)NC}$_3$Cr(CN)$_3$][10c] containing

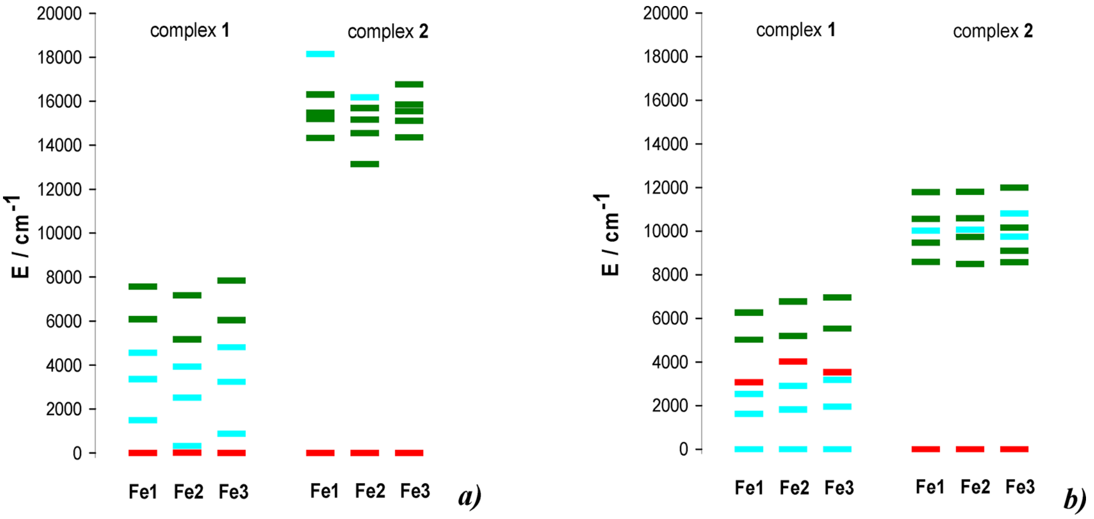

Figure 5. Electronic terms of the central atoms of complexes **1** (left) and **2** (right) calculated with (a) the SA-CAS[5,5]SCF+NEVPT2 method and (b) the SA-CAS[9,12]SCF+NEVPT2 method. Spin doublets, blue; spin quartets, green; spin sextets, red.

Table 5. Calculated Magnetic Parameters of Fe(III) Centers

complex/center	D (cm^{-1})[a]	E/D[a]	g[a]	J (cm^{-1})[b]
1/Fe1	–	–	2.287	–
1/Fe2	–	–	2.270	–
1/Fe3	–	–	2.260	–
2/Fe1	0.4843	0.2021	1.998	0.0013 (between Fe1 and Fe2)
2/Fe2	0.4256	0.0394	1.998	−0.0197 (between Fe2 and Fe3)
2/Fe3	±0.4854	0.3271	1.998	0.0573 (between Fe3 and Fe1)

[a] SA-CAS[9,12]SCF+NEVPT2. [b] B3LYP.

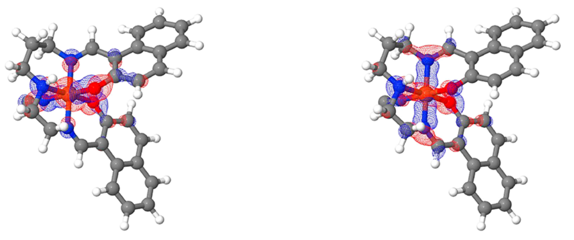

a) MO 128, occupancy number 1.9661

b) MO 129, occupancy number 1.9565

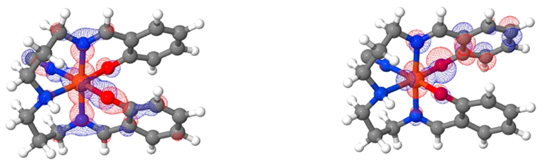

c) MO 106, occupancy number 1.9770

d) MO 107, occupancy number 1.7804

Figure 6. Bonding active orbitals e_g of center Fe2 in **1**, (a) MO127 and (b) MO128. Bonding active orbitals e_g of Fe2 in **2**, (c) MO106 and (d) MO107.

the paramagnetic hexacyanidochromate(III) bridging backbone (Figure S7a). In this case, {Fe(L2)} complex units are arranged in a meridional-like fashion that afforded the T shape of the whole molecule. That compound shows a half-complete thermal SCO with 50% of the Fe(III) in the HS state permanently. The single-crystal X-ray structure determined at 185 K, with ~60% of the Fe(III) atoms in the HS state, has been used for the calculations. Bonding e_g orbital 107 in [{Fe(L2)NC}$_3$Cr(CN)$_3$] is displaced similarly like that in compound **2** (Figure S7b), which leads to the tentative conclusion that the delocalized e_g orbitals in **2** and [{Fe(L2)-NC}$_3$Cr(CN)$_3$] are more likely to accommodate the unpaired electron than the localized one in **1**. One can thus assume that such delocalization stays at the core of the stabilization of the HS state. This hypothesis can explain the strikingly high sensitivity of studied SCO systems with respect to their subtle structural modifications, polymorphism, and solvatomorphism.

■ CONCLUSION

Two novel tetranuclear neutral complexes consisting of three paramagnetic Fe(III) metal centers and one diamagnetic Co(III) metal center were prepared, and their structural and magnetic properties were investigated in detail. SB ligands used for the preparation of both complexes contain different aromatic as well as aliphatic parts, which obviously affect the magnetism of both isostructural analogues. The first complex **1** with a SB ligand containing an asymmetric aliphatic bridge and two naphthalene aromatic moieties shows LS behavior in its solvated form and hysteretic SCO in its desolvated form. On the other hand, employing the SB ligand with symmetric aliphatic and phenolic aromatic parts for the preparation of the second tetranuclear complex results in the observation of permanent HS state behavior in **2**, which is independent of the presence of lattice solvent molecules in the crystal structure. The structural and magnetic properties of **1** and **2** can be also discussed in comparison with those of the previously reported tetranuclear complex [{Fe(L2)NC}$_3$Cr(CN)$_3$] exhibiting half-complete thermal SCO where 50% of Fe(III) remains in the HS state permanently.[10c] It appears that the type of coordination center of the used hexacyanidometalate anions controls the spatial arrangement of the ferric complex units coordinated on $[M(CN)_6]^{3-}$, because both compounds reported herein with a diamagnetic Co(III) ion adopt a facial-like coordination contrary to the T-shaped molecule $[\{Fe(L2)NC\}_3Cr(CN)_3]$ with a meridional-like alignment of {Fe(L2)} moieties. SA-CASSCF+NEVPT2 calculation with a large active space of nine electrons in 12 orbitals reproduced correctly the ground spin state on individual Fe(III) centers and suggested that the spin state was governed by the delicate arrangement of the ligand, especially its secondary structure involving the aromatic rings. One can thus conclude that the similar delocalization of bonding e_g orbitals in compounds **2** and $[\{Fe(L2)NC\}_3Cr(CN)_3]$ containing the same pentadentate ligand $L2^{2-}$ possesses an effectively weaker ligand field compared to that of $L1^{2-}$ stabilizing the permanent HS state in **2**. On the other hand, $L1^{2-}$ stabilizes the LS state and incomplete SCO in the solvated and desolvated forms of **1**, respectively. Indeed, a similar conclusion stating that twisted ligand conformations displacing the ligand lone pairs from the metal−ligand vector weaken the ligand field in the complexes was drawn elsewhere for a specific class of Fe(II) SCO complexes.[19] In conclusion, one can speculate that SCO in system **2** is not hindered by the intermolecular strain; rather, the ligands do not provide a suitable ligand field. On the contrary, the ligands of system **1** support SCO behavior that can be further modulated by intermolecular interactions.

■ EXPERIMENTAL SECTION

General. All purchased chemicals and solvents were used as received. Methanol, acetonitrile, and diethyl ether were used as solvents without further purification. Potassium hexacyanidocobaltate $K_3[Co(CN)_6]$ was prepared as previously described.[20] Elemental analysis of carbon, hydrogen, and nitrogen was carried out by an automated analyzer (Vario, Micro Cube). IR spectra were measured by the ATR technique or in KBr pellets in the range of 4000−400 cm^{-1} (Magna FTIR 750, Nicolet). TG-DTA analysis was performed in a He flow at a heating rate of 2.5 K min^{-1} in a Netzsch STA 409 C analyzer.

Synthesis of Complexes. *Mononuclear Complexes [Fe(L1)Cl] and [Fe(L2)Cl].* The synthesis of mononuclear complexes [Fe(L1)Cl] and [Fe(L2)Cl] was adapted according to a previously reported procedure.[8,21] A methanol solution (20 cm^3) of the corresponding carbaldehyde (2 equiv of salicylaldehyde for [Fe(L1)Cl]; 2 equiv of 2-hydroxynaphthaldehyde for [Fe(L2)Cl]) was combined with aliphatic triamine (1 equiv of *N*-(2-aminoethyl)-1,3-propanediamine for [Fe(L1)Cl]; 1 equiv of bis(3-aminopropyl)amine for [Fe(L2)Cl]) dissolved in 10 cm^3 of CH_3OH, and the reaction mixture was stirred at 40 °C for 30 min. Then, 1 equiv of $FeCl_3·6H_2O$ in 10 cm^3 of CH_3OH was added to the *in situ*-prepared Schiff base (H_2L1 or H_2L2), which afforded formation of the desired mononuclear complex. The mixture was stirred at 60 °C to evaporate $^1/_3$ of the volume and cooled to −10 °C, and a dark polycrystalline powder was separated by filtration under vacuum, washed with several portions of cold CH_3OH and diethyl ether, and dried. Elemental Anal. [Fe(L1)Cl] found (calcd) for $C_{20}H_{23}ClFeN_3O_2$ (428.71 g/mol): C, 55.88% (56.03%); H, 5.22% (5.41%); N, 9.72% (9.80%). [Fe(L2)Cl] found (calcd) for $C_{27}H_{25}ClFeN_3O_2$ (514.80 g/mol): C, 62.87% (62.99%); H, 4.80% (4.89%); N, 8.01% (8.16%).

*Synthesis of **1** ($[\{Fe(L1)NC\}_3Co(CN)_3]·2CH_3OH·2.5CH_3CN$).* [Fe(L1)Cl] (0.3 g, 0.7 mmol, 3 equiv) was dissolved in 120 cm^3 of acetonitrile and methanol (1:1) and combined with solid potassium hexacyanocobaltate $K_3[Co(CN)_6]$ (64 mg, 0.19 mmol, 3 equiv). The reaction mixture was refluxed for 24 h at 70 °C, cooled to room temperature, and filtered, and the volume of the solvents was reduced under vacuum by half. Small dark green crystals were collected after slow crystallization at 5 °C for 2 weeks. Yield: 90 mg (0.048 mmol, 25%). Elemental Anal. Found (calcd) for $C_{94}H_{90.50}CoFe_3N_{17.50}O_8$ (M_w = 1819.81 g mol^{-1}): C, 60.85% (62.04%); N, 13.01% (13.47%); H, 4.95% (5.01%). FT-IR (KBr): 3405(s) (OH), 3224(w), 3062(w) (C_{ar}−H), 2947(w) (C_{al}−H), 2876(w) (C_{al}−H), 2166(m) (C≡N), 2128(s) (C≡N), 1617(s) (C_{ar}−C_{ar} and C═N), 1603(s) (C_{ar}−C_{ar} and C═N), 1541(s) (C_{ar}−C_{ar} and C═N), 1509(w) (C_{ar}−C_{ar} and C═N).

*Synthesis of **2** ($[\{Fe(L2)NC\}_3Co(CN)_3]·CH_3OH·2H_2O$).* $K_3[Co(CN)_6]$ (77 mg, 0.23 mmol, 3 equiv) was added to 40 cm^3 of a methanolic solution of mononuclear complex [Fe(L2)Cl] (0.3 g, 0.70 mmol, 3 equiv), and the reaction mixture was refluxed overnight at 70 °C. The resulting solution was filtered off and subjected to slow crystallization at 5 °C, which allowed formation of dark violet crystals after a couple of days. Yield: 55 mg (0.037 mmol, 31%). Elemental Anal. Found (calcd) for $C_{67}H_{77}CoFe_3N_{15}O_9$ (M_w = 1462.92 g mol^{-1}): C, 53.95% (55.01%); N, 13.48% (14.36%); H, 5.05% (5.31%). FT-IR (KBr): 3406 (OH), 2931 (C−H), 2177, 2162, 2156, 2141 (C≡N), 1620 (C═N).

Crystal Structure Determination. Single-crystal X-ray diffraction data of **1** were collected on a STOE IPDS2T diffractometer with monochromated Mo Kα (0.71073 Å) radiation at low temperatures. Using Olex2,[22] the structures were determined with the ShelXS[23] structure solution program using direct methods and refined with the ShelXL[24] refinement package using least-squares minimization. Refinement was performed with anisotropic temperature factors for all non-hydrogen atoms (disordered atoms and solvent molecules were refined isotropically); hydrogen atoms were calculated at idealized positions. Single-crystal X-ray diffraction data of **2** were collected using an Oxford diffraction Xcalibur diffractometer with a Sapphire CCD detector installed in a fine-focus sealed tube (Mo Kα radiation; λ = 0.71073 Å) and equipped with an Oxford Cryosystems nitrogen gas-flow apparatus. The structure was determined with the ShelXs software using direct methods and refined using least-squares minimization with the ShelXL software[24] incorporated in the Wingx package.[25] For each structure, its space group was checked by the ADSYMM procedure of the PLATON software.[26] All non-hydrogen atoms were refined anisotropically. The hydrogen atoms were placed into the calculated positions and included in the riding-model approximation with a U_{iso} of 1.2U_{eq} or 1.5U_{eq} (atom of attachment).

Nonroutine aspects of the structural refinement are as follows. In **1**, the measured crystals exhibited poor diffraction power. This, together with the relatively large unit cell of **1**, affected collection of large-angle diffractions and resulted in lower completeness of the data. The aliphatic part of the ligand in one of the {Fe(L1)NC} fragments is disordered over two positions. While it was possible to model disorder for the more rigid ethyl part, it was not possible to establish it for the longer propyl part. The measured crystals suffered from partial solvent loss, which resulted in lower occupation parameters (0.5), which were used to reasonably model co-crystallized methanol molecules. The acetonitrile molecules were also affected; however, it was possible to model them using SADI/EADP constraints and restraints. In **2**, the electron density corresponding to heavily disordered superimposed molecules of water and methanol was left unmodeled, because it was not possible to establish a reasonable model. Attempts to use the SQUEEZE procedure[27] to remove this electron density resulted in an R_1 much lower than that reported for the structure presented herein, but the goodness of fit fell below 0.8. Therefore, we decided not to use "squeezed" data.

Magnetic Measurements. Magnetic investigations were performed by using a SQUID magnetometer (MPMS-XL7, Quantum Design) in the RSO mode of detection. In all cases, the temperature dependence of the magnetic moment was recorded at 0.1 T as an external magnetic field and the temperature sweeping rate was 1 K/min. Desolvation of compounds **1** and **2** was performed *in situ* within the magnetic measurement setup. After the first heating, three continuous cooling/heating cycles were applied until the last two measurements were identical. Thereby, the sample was maintained in the MPMS magnetometer at 380 K for 20 min before every cooling/heating cycle. The gelatin-made capsules were used as sample holders, and their small diamagnetic contribution made a negligible contribution to the overall magnetization, which was dominated by the sample. The diamagnetic corrections to the molar magnetic susceptibilities were applied using Pascal constants.[28]

Computational Details. The fitting of the magnetic susceptibility and magnetization in **2** was performed with PHI 3.1.1,[29] and the spin crossover transition curve in the case of **1** with a homemade program.[30]

The geometry of the complete molecule **1** was optimized with the help of Gaussian 16 revision b.01[43] in two steps. In the first step, the geometry was optimized using the meta-GGA functional TPSS[44] and the Ahlrichs' basis set STO-3G[45] for all atoms. In the second step, the obtained geometry was refined with meta-hybrid functional TPSSh[44] and higher-quality basis set 3-21G for iron atoms.[46] To account for the intermolecular interactions, the empirical dispersion correction D3BJ was employed during all calculations.[47] No imaginary frequencies were found for any of resulting geometries.

Calculations of magnetic parameters were carried out within ORCA 4.0.1.[31] The zero-field splitting (ZFS) parameters and crystal field term energies were obtained using the state-averaged complete active space self-consistent field method[32] (SA-CAS[5,5]SCF and SA-CAS[9,12]SCF) complemented by strongly contracted N-electron valence perturbation theory of second order (NEVPT2).[33] In either case, one spin sextet reference state, 24 spin quartet reference states, and 60 spin doublet reference states were taken into account. The second-order Douglass−Kroll−Hess correction (DKH2)[34] and the chain-of-spheres approximation (RIJCOSX)[35] were set on. For all atoms, the relativistically recontracted Ahlrichs' basis DKH-def2-TZVP[36] was used with an automatically generated auxiliary basis set.[37] Prior to this calculation, the positions of all hydrogen atoms were optimized on the model fragments using the method PBEh-3c[38] and all other atoms were kept in their positions as obtained from the X-ray analysis. The ZFS parameters were calculated by quasi-degenerate perturbation theory (QDPT),[39] in which an approximation to the Breit−Pauli form of the spin−orbit coupling operator (SOMF approximation)[40] and the effective Hamiltonian theory were utilized.[41] The magnetic exchange parameters were obtained from DFT calculation utilizing the same basis, RIJCOSX approximation, and hybrid functional B3LYP.[42] In all calculations, the increased integration grid was used (level 4 in ORCA convention).

■ ASSOCIATED CONTENT

Supporting Information

The Supporting Information is available free of charge at https://pubs.acs.org/doi/10.1021/acs.inorgchem.9b03097.

> Computational details and magnetic measurements at static and dynamic magnetic fields (PDF)

Accession Codes

CCDC 1869404 and 1954726 contain the supplementary crystallographic data for this paper. These data can be obtained free of charge via www.ccdc.cam.ac.uk/data_request/cif, or by emailing data_request@ccdc.cam.ac.uk, or by contacting The Cambridge Crystallographic Data Centre, 12 Union Road, Cambridge CB2 1EZ, UK; fax: +44 1223 336033.

■ AUTHOR INFORMATION

Corresponding Author

Ivan Šalitroš − *Department of Inorganic Chemistry, Faculty of Chemical and Food Technology, Slovak University of Technology in Bratislava, Bratislava SK-81237, Slovakia; Central European Institute of Technology, Brno University of Technology, 61200 Brno, Czech Republic; Department of Inorganic Chemistry, Faculty of Science, Palacký University, 771 46 Olomouc, Czech Republic;* orcid.org/0000-0003-3856-0399; Email: ivan.salitros@stuba.sk

Authors

Ján Pavlik − *Department of Inorganic Chemistry, Faculty of Chemical and Food Technology, Slovak University of Technology in Bratislava, Bratislava SK-81237, Slovakia*

Petra Masárová − *Department of Inorganic Chemistry, Faculty of Chemical and Food Technology, Slovak University of Technology in Bratislava, Bratislava SK-81237, Slovakia*

Ivan Nemec − *Central European Institute of Technology, Brno University of Technology, 61200 Brno, Czech Republic; Department of Inorganic Chemistry, Faculty of Science, Palacký University, 771 46 Olomouc, Czech Republic;* orcid.org/0000-0003-3231-7849

Olaf Fuhr − *Institut für Nanotechnologie, Karlsruher Institut für Technologie, Karlsruhe 76021, Germany; Karlsruhe Nano Micro Facility (KNMF), Karlsruher Institut für Technologie, Karlsruhe 76021, Germany*

Mario Ruben − *Institut für Nanotechnologie, Karlsruher Institut für Technologie, Karlsruhe 76021, Germany; Institute de Physique et Chimie de Matériaux de Strasbourg (IPCMS), CNRS-Université de Strasbourg, 67034 Strasbourg, France*

Complete contact information is available at: https://pubs.acs.org/10.1021/acs.inorgchem.9b03097

Notes

The authors declare no competing financial interest.

■ ACKNOWLEDGMENTS

Slovak grant agencies (APVV-18-0197, APVV-18-0016, and VEGA 1/0125/18) and the Ministry of Education, Youth and Sports of the Czech Republic under Project CEITEC 2020 (LQ1601) are acknowledged for financial support. I.Š. and I.N. acknowledge the financial support from institutional sources of the Department of Inorganic Chemistry, Palacký University Olomouc. The authors are also grateful to the HPC center at the Slovak University of Technology in Bratislava, which is a part of the Slovak Infrastructure of High Performance Computing [SIVVP project, ITMS code 26230120002, funded by the European region development funds (ERDF)].

■ REFERENCES

(1) See reviews and references therein:(a) Halcrow, M. A., Ed. *Spin-Crossover Materials, Properties and Applications*; Wiley: Hoboken, NJ, 2013. (b) van Koningsbruggen, P. J.; Maeda, Y.; Oshio, H. Iron(III) spin crossover compounds. *Top. Curr. Chem.* **2004**, *233*, 259−324. (c) Harding, D. J.; Harding, P.; Phonsri, W. Spin crossover in iron(III) complexes. *Coord. Chem. Rev.* **2016**, *313*, 38−61.

(2) (a) Oshio, H.; Kitazaki, K.; Mishiro, K. J.; Kato, N.; Maeda, Y.; Takashima, Y. New spin-crossover iron(III) complexes with large hysteresis effects and time dependence of their magnetism. *J. Chem. Soc., Dalton Trans.* **1987**, *6*, 1341−1347. (b) Nakaya, M.; Shimayama, K.; Takami, K.; Hirata, K.; Alao, A. S.; Nakamura, M.; Lindoy, L. F.; Hayami, S. Spin-crossover and LIESST Effect for Iron(III) Complex Based on π−π Stacking by Coordination Programming. *Chem. Lett.* **2014**, *43* (7), 1058−1060. (c) Iasco, O.; Rivière, E.; Guillot, R.; Buron-Le Cointe, M.; Meunier, J.-F.; Bousseksou, A.; Boillot, M.-L. FeII(pap-5NO2)2 and FeII(qsal-5NO2)2 Schiff-Base Spin-Crossover Complexes: A Rare Example with Photomagnetism and Room-Temperature Bistability. *Inorg. Chem.* **2015**, *54* (4), 1791−1799. (cc) Martins, F. F.; Joseph, A.; Diogo, H. P.; Minas da Piedade, M. E.; Ferreira, L. P.; Carvalho, M. D.; Barroso, S.; Romão, M. J.; Calhorda, M. J.; Martinho, P. N. Irreversible Magnetic Behaviour Caused by the Thermosalient Phenomenon in an Iron(III) Spin Crossover Complex. *Eur. J. Inorg. Chem.* **2018**, *2018*, 2976−2983. (d) Liu, X.; Hamon, J.-R. Recent developments in penta-, hexa- and heptadentate Schiff base

ligands and their metal complexes. *Coord. Chem. Rev.* **2019**, *389* (15), 94−118.

(3) (a) Imatomi, S.; Hashimoto, S.; Matsumoto, N. Inter- and Intrachain Spin-Transition Processes in One-Dimensional Polynuclear Iron(III) Complexes of N,N′-Ethylenebis (acetylacetonylideneimine) Bridged by 1,3- Bis (4-pyridyl) propane and 1,4-Bis-(imidazolyl)butane. *Eur. J. Inorg. Chem.* **2009**, *2009*, 721−726. (b) Ross, T. M.; Neville, S. M.; Innes, D. S.; Turner, D. R.; Moubaraki, B.; Murray, K. S. Spin crossover in iron(III) Schiff-base 1-D chain complexes. *Dalton Trans.* **2010**, *39* (1), 149−159.

(4) (a) Shen, X.-P.; Xu, Z.; Yuan, A.-H.; Huang, Z.-X. Syntheses, crystal structures and magnetic properties of two cyano-bridged two-dimensional assemblies [Fe(salpn)]2[Fe(CN)5NO] and [Fe(salpn)]-2[Ni(CN)4]. *Transition Met. Chem.* **2004**, *29*, 100−106. (b) Re, N.; Crescenzi, R.; Floriani, C.; Miyasaka, H.; Matsumoto, N. The Synthesis and Characterization of Two-Dimensional Ferromagnetic Extended Structures Containing High-Spin (S = 5/2) and Low-Spin (S = 1/2) Iron(III) Bridged by Cyanide Groups. *Inorg. Chem.* **1998**, *37* (11), 2717−2722.

(5) Yang, Z.; Zhu, C.; Li, Z.; Liu, Y.; Liu, G.; Cui, Y. Engineering chiral Fe(salen)-based metal−organic frameworks for asymmetric sulfide oxidation. *Chem. Commun.* **2014**, *50*, 8775−8778.

(6) Chorazy, S.; Stanek, J. J.; Kobylarczyk, J.; Ohkoshi, S.; Sieklucka, B.; Podgajny, R. Modulation of the FeII spin crossover effect in the pentadecanuclear {Fe9[M(CN)8]6} (M = Re, W) clusters by facial coordination of tridentate polyamine ligands. *Dalton Trans.* **2017**, *46*, 8027−8036.

(7) Boča, R.; Šalitroš, I.; Kožíšek, J.; Linares, J.; Moncoĺ, J.; Renz, F. Spin crossover in a heptanuclear mixed-valence iron complex. *Dalton Trans.* **2010**, *39*, 2198−2200.

(8) (a) Rogez, G.; Marvilliers, A.; Riviére, E.; Audiére, J. P.; Lloret, F.; Varret, F.; Goujon, A.; Mendenez, N.; Girerd, J. J.; Mallah, T. A Mixed-Valence Mixed-Spin Prussian-Blue-Like Heptanuclear Complex. *Angew. Chem., Int. Ed.* **2000**, *39* (16), 2885−2887. (b) Rogez, G.; Parsons, S.; Paulsen, C.; Villar, V.; Mallah, T. A Prussian Blue Nanomolecule: Crystal Structure and Low-Temperature Magnetism. *Inorg. Chem.* **2001**, *40* (16), 3836−3837. (c) Gembický, M.; Boča, R.; Renz, F. A heptanuclear Fe(II)−Fe(III)6 system with twelve unpaired electrons. *Inorg. Chem. Commun.* **2000**, *3* (11), 662−665. (d) Šalitroš, I.; Boča, R.; Herchel, R.; Moncoĺ, J.; Nemec, I.; Ruben, M.; Renz, F. Mixed-Valence Heptanuclear Iron Complexes with Ferromagnetic Interaction. *Inorg. Chem.* **2012**, *51* (23), 12755−12767.

(9) Glaser, T.; Heidemeier, M.; Weyhermuller, T.; Hoffmann, R.-D.; Rupp, H.; Muller, P. Property-Oriented Rational Design of Single-Molecule Magnets: A C3-Symmetric Mn6Cr Complex based on Three Molecular Building Blocks with a Spin Ground State of S = 21/2. *Angew. Chem., Int. Ed.* **2006**, *45* (36), 6033−6037.

(10) (a) Zhang, Y.-Z.; Wang, B. W.; Sato, O.; Gao, S. First Fe(ii)-based cyano-bridged single molecule magnet [CrIIIFeII2] with a large anisotropy. *Chem. Commun.* **2010**, *46* (37), 6959−6961. (b) Shatruk, M.; Dragulescu-Andrasi, A.; Chambers, K. E.; Stoian, S. A.; Bominaar, E. L.; Achim, C.; Dunbar, K. R. Properties of Prussian Blue Materials Manifested in Molecular Complexes: Observation of Cyanide Linkage Isomerism and Spin-Crossover Behavior in Pentanuclear Cyanide Clusters. *J. Am. Chem. Soc.* **2007**, *129* (19), 6104−6116. (c) Herchel, R.; Boča, R.; Gembický, M.; Kožíšek, J.; Renz, F. Spin Crossover in a Tetranuclear Cr(III)-Fe(III)3 Complex. *Inorg. Chem.* **2004**, *43* (14), 4103−4105.

(11) (a) Pogány, L.; Moncoĺ, J.; Pavlik, J.; Mazúr, M.; Šalitroš, I. High-Spin Mononuclear Iron(III) Complexes with Pentadentate Schiff Base Ligands: Structural Analysis and Magnetic Properties. *ChemPlusChem* **2019**, *84* (4), 358−367. (b) Pogány, L.; Brachňaková, B.; Masárová, P.; Moncoĺ, J.; Pavlik, J.; Gál, M.; Mazúr, M.; Herchel, R.; Nemec, I.; Šalitroš, I. Impact of the Schiff base ligand substituents on the solid state and solution properties of eleven iron(iii) complexes. *New J. Chem.* **2019**, *43* (35), 13916−13928. (c) Pogány, L.; Brachňaková, B.; Moncoĺ, J.; Pavlik, J.; Nemec, I.; Trávníček, Z.; Mazúr, M.; Bučinský, L.; Suchánek, L.; Šalitroš, I. Impact of Substituent Variation on the Presence of Thermal Spin Crossover in a Series of Mononuclear Iron(III) Schiff Base Complexes with Terminal Pseudohalido Co-ligands. *Chem. - Eur. J.* **2018**, *24* (20), 5191−5203. (d) Pogány, L.; Masárová, P.; Moncoĺ, J.; Pavlik, J.; Šalitroš, I. Series of high spin mononuclear iron(iii) complexes with Schiff base ligands derived from 2-hydroxybenzophenones. *New J. Chem.* **2017**, *41* (13), 5904−5915. (e) Nemec, I.; Herchel, R.; Boča, R.; Trávniček, Z.; Svoboda, I.; Fuess, H.; Linert, W. Tuning of spin crossover behaviour in iron(iii) complexes involving pentadentate Schiff bases and pseudohalides. *Dalton Trans.* **2011**, *40* (39), 10090−10099.

(12) $\Sigma = \Sigma_{i-1}{}^{12}(|\varphi_1 - 90|)$, where φ_1 is value of the N−Fe−N octahedron angle. Adapted from: (a) Guionneau, P.; Marchivie, M.; Bravic, G.; Létard, J. F.; Chasseau, D. Structural Aspects of Spin Crossover. Example of the [FeIILn(NCS)2] Complexes. *Top. Curr. Chem.* **2004**, *234*, 97−128. $\Theta = \Theta_{i-1}{}^{12}(|\theta_i - 90|)$, where θ_i values are 24 angles measured on the projection of two triangular faces of the octahedron along with their common pseudo-three-fold axis. Adapted from: (b) Halcrow, M. A. Structure: function relationships in molecular spin-crossover complexes. *Chem. Soc. Rev.* **2011**, *40* (7), 4119−4142.

(13) (a) Alvarez, S.; Avnir, D.; Llunell, M.; Pinsky, M. Continuous symmetry maps and shape classification. The case of six-coordinated metal compounds. *New J. Chem.* **2002**, *26* (8), 996−1009. (b) Alvarez, S. Relationships between Temperature, Magnetic Moment, and Continuous Symmetry Measures in Spin Crossover Complexes. *J. Am. Chem. Soc.* **2003**, *125* (22), 6795−6802. (c) Alvarez, S. Distortion Pathways of Transition Metal Coordination Polyhedra Induced by Chelating Topology. *Chem. Rev.* **2015**, *115* (24), 13447−13483.

(14) (a) Pavlik, J.; Linares, J. Microscopic models of spin crossover. *C. R. Chim.* **2018**, *21* (12), 1170−1178. (b) Pavlik, J.; Boča, R. Established Static Models of Spin Crossover. *Eur. J. Inorg. Chem.* **2013**, *2013*, 697−709.

(15) (a) Bousseksou, A.; Constant-Machado, H.; Varret, F. A Simple Ising-Like Model for Spin Conversion Including Molecular Vibrations. *J. Phys. I* **1995**, *5* (6), 747−760. (b) Tuchagues, J.-P.; Bousseksou, A.; Molnár, G.; McGarvey, J. J.; Varret, F. The Role of Molecular Vibrations in the Spin Crossover Phenomenon. *Top. Curr. Chem.* **2004**, *235*, 84−103.

(16) Boča, R. Zero-field splitting in metal complexes. *Coord. Chem. Rev.* **2004**, *248* (9−10), 757−815.

(17) (a) Nemec, I.; Svoboda, I.; Herchel, R. *Metals* **2019**, *9* (8), 849. (b) Cirera, J.; Via-Nadal, M.; Ruiz, E. Benchmarking Density Functional Methods for Calculation of State Energies of First Row Spin-Crossover Molecules. *Inorg. Chem.* **2018**, *57* (22), 14097−14105. (c) Siig, O. S.; Kepp, K. P. Iron(II) and Iron(III) Spin Crossover: Toward an Optimal Density Functional. *J. Phys. Chem. A* **2018**, *122* (16), 4208−4217. (d) Kepp, K. P. Theoretical Study of Spin Crossover in 30 Iron Complexes. *Inorg. Chem.* **2016**, *55* (6), 2717−2727. Mortensen, S. R.; Kepp, K. P. Spin Propensities of Octahedral Complexes From Density Functional Theory. *J. Phys. Chem. A* **2015**, *119* (17), 4041−4050.

(18) (a) Saureu, S.; de Graaf, C. TD-DFT study of the light-induced spin crossover of Fe(iii) complexes. *Phys. Chem. Chem. Phys.* **2016**, *18* (2), 1233−1244. (b) Pierloot, K.; Vancoillie, S. Relative energy of the high and low spin states of [Fe(H2O)6]2+, [Fe(NH3)6]2+, and [Fe(bpy)3]2+: CASPT2 versus density functional theory. *J. Chem. Phys.* **2006**, *125* (12), 124303.

(19) Halcrow, M. A. The Effect of Ligand Design on Metal Ion Spin State—Lessons from Spin Crossover Complexes. *Crystals* **2016**, *6* (5), 58.

(20) Brauer, G., Ed.; *Handbook of preparative inorganic chemistry*; Academic Press: New York, 1963.

(21) CCDC SIMPFE: Holt, E. M.; Holt, S. L.; Vlasse, M. *Cryst. Struct. Commun.* **1979**, *8*, 645.

(22) Dolomanov, O. V.; Bourhis, L. J.; Gildea, R. J.; Howard, J. A. K.; Puschmann, H. OLEX2: a complete structure solution, refinement and analysis program. *J. Appl. Crystallogr.* **2009**, *42*, 339−341.

(23) Sheldrick, G. M. A short history of SHELX. *Acta Crystallogr., Sect. A: Found. Crystallogr.* **2008**, *A64*, 112−122.

(24) Sheldrick, G. M. Crystal structure refinement with SHELXL. *Acta Crystallogr., Sect. C: Struct. Chem.* **2015**, *C71*, 3−8.

(25) Macrae, C. F.; Edgington, P. R.; McCabe, P.; Pidcock, E.; Shields, G. P.; Taylor, R.; Towler, M.; van de Streek, J. Mercury: visualization and analysis of crystal structures. *J. Appl. Crystallogr.* **2006**, *39*, 453−457.

(26) Speck, A. L. *PLATON, a multipurpose crystallographic tool*; Utrecht University: Utrecht, The Netherlands, 2001. (b) Le Page, Y. MISSYM1.1 − a flexible new release. *J. Appl. Crystallogr.* **1988**, *21*, 983.

(27) Spek, A. L. PLATON SQUEEZE: a tool for the calculation of the disordered solvent contribution to the calculated structure factors. *Acta Crystallogr., Sect. C: Struct. Chem.* **2015**, *71*, 9−18.

(28) Boča, R. *Theoretical Foundations of Molecular Magnetism*; Elsevier: Amsterdam, 1999.

(29) Chilton, N. F.; Anderson, R. P.; Turner, L. D.; Soncini, A.; Murray, K. S. PHI: a powerful new program for the analysis of anisotropic monomeric and exchange-coupled polynuclear d- and f-block complexes. *J. Comput. Chem.* **2013**, *34* (13), 1164−1175.

(30) Boča, R. *POLYMAGNET*; University of SS. Cyril and Methodius: Trnava, Slovakia, 2013.

(31) Neese, F. Software update: the ORCA program system, version 4.0. *Wiley Interdisciplinary Reviews: Computational Molecular Science* **2018**, *8* (1), e1327.

(32) Malmqvist, P. A.; Roos, B. O. The CASSCF state interaction method. *Chem. Phys. Lett.* **1989**, *155* (2), 189−194.

(33) (a) Angeli, C.; Cimiraglia, R.; Malrieu, J.-P. N-electron valence state perturbation theory: a fast implementation of the strongly contracted variant. *Chem. Phys. Lett.* **2001**, *350* (3−4), 297−305. (b) Angeli, C.; Cimiraglia, R.; Evangelisti, S.; Leininger, T.; Malrieu, J.-P. Introduction of n-electron valence states for multireference perturbation theory. *J. Chem. Phys.* **2001**, *114* (23), 10252−10264. (c) Angeli, C.; Cimiraglia, R.; Malrieu, J.-P. N-electron valence state perturbation theory: A spinless formulation and an efficient implementation of the strongly contracted and of the partially contracted variants. *J. Chem. Phys.* **2002**, *117* (20), 9138−9153.

(34) Nakajima, T.; Hirao, K. The Douglas−Kroll−Hess Approach. *Chem. Rev.* **2012**, *112* (1), 385−402.

(35) Izsak, R.; Neese, F. An overlap fitted chain of spheres exchange method. *J. Chem. Phys.* **2011**, *135* (14), 144105.

(36) Weigend, F.; Ahlrichs, R. Balanced basis sets of split valence, triple zeta valence and quadruple zeta valence quality for H to Rn: Design and assessment of accuracy. *Phys. Chem. Chem. Phys.* **2005**, *7* (18), 3297−3305.

(37) Stoychev, G. L.; Auer, A. A.; Neese, F. Automatic Generation of Auxiliary Basis Sets. *J. Chem. Theory Comput.* **2017**, *13* (2), 554−562.

(38) Grimme, S.; Brandenburg, J. G.; Bannwarth, C.; Hansen, A. Consistent structures and interactions by density functional theory with small atomic orbital basis sets. *J. Chem. Phys.* **2015**, *143* (5), 054107.

(39) Ganyushin, D.; Neese, F. First-principles calculations of zero-field splitting parameters. *J. Chem. Phys.* **2006**, *125* (2), 024103.

(40) Neese, F. Efficient and accurate approximations to the molecular spin-orbit coupling operator and their use in molecular g-tensor calculations. *J. Chem. Phys.* **2005**, *122* (3), 034107.

(41) Maurice, R.; Bastardis, R.; de Graaf, C.; Suaud, N.; Mallah, T.; Guihéry, N. Universal Theoretical Approach to Extract Anisotropic Spin Hamiltonians. *J. Chem. Theory Comput.* **2009**, *5* (11), 2977−2984.

(42) (a) Lee, C.; Yang, W.; Parr, R. G. Development of the Colle-Salvetti correlation-energy formula into a functional of the electron density. *Phys. Rev. B: Condens. Matter Mater. Phys.* **1988**, *37* (2), 785−789. (b) Becke, A. D. Density-functional thermochemistry. III. The role of exact exchange. *J. Chem. Phys.* **1993**, *98* (7), 5648−5651. (c) Vosko, S. H.; Wilk, L.; Nusair, M. Accurate spin-dependent electron liquid correlation energies for local spin density calculations: a critical analysis. *Can. J. Phys.* **1980**, *58* (8), 1200−1211. (d) Stephens, P. J.; Devlin, F. J.; Chabalowski, C. F.; Frisch, M. J. Ab Initio Calculation of Vibrational Absorption and Circular Dichroism Spectra Using Density Functional Force Fields. *J. Phys. Chem.* **1994**, *98* (45), 11623−11627.

(43) Frisch, M. J.; Trucks, G. W.; Schlegel, H. B.; Scuseria, G. E.; Robb, M. A.; Cheeseman, J. R.; Scalmani, G.; Barone, V.; Petersson, G. A.; Nakatsuji, H.; Li, X.; Caricato, M.; Marenich, A. V.; Bloino, J.; Janesko, B. G.; Gomperts, R.; Mennucci, B.; Hratchian, H. P.; Ortiz, J. V.; Izmaylov, A. F.; Sonnenberg, J. L.; Williams-Young, D.; Ding, F.; Lipparini, F.; Egidi, F.; Goings, J.; Peng, B.; Petrone, A.; Henderson, T.; Ranasinghe, D.; Zakrzewski, V. G.; Gao, J.; Rega, N.; Zheng, G.; Liang, W.; Hada, M.; Ehara, M.; Toyota, K.; Fukuda, R.; Hasegawa, J.; Ishida, M.; Nakajima, T.; Honda, Y.; Kitao, O.; Nakai, H.; Vreven, T.; Throssell, K.; Montgomery, J. A., Jr.; Peralta, J. E.; Ogliaro, F.; Bearpark, M. J.; Heyd, J. J.; Brothers, E. N.; Kudin, K. N.; Staroverov, V. N.; Keith, T. A.; Kobayashi, R.; Normand, J.; Raghavachari, K.; Rendell, A. P.; Burant, J. C.; Iyengar, S. S.; Tomasi, J.; Cossi, M.; Millam, J. M.; Klene, M.; Adamo, C.; Cammi, R.; Ochterski, J. W.; Martin, R. L.; Morokuma, K.; Farkas, O.; Foresman, J. B.; Fox, D. J. *Gaussian 16*, revision b.01; Gaussian, Inc.: Wallingford, CT, 2016.

(44) Tao, J. M.; Perdew, J. P.; Staroverov, V. N.; Scuseria, G. E. Climbing the Density Functional Ladder: Nonempirical Meta−Generalized Gradient Approximation Designed for Molecules and Solids. *Phys. Rev. Lett.* **2003**, *91* (14), 146401.

(45) (a) Hehre, W. J.; Stewart, R. F.; Pople, J. A. Self-Consistent Molecular-Orbital Methods. I. Use of Gaussian Expansions of Slater-Type Atomic Orbitals. *J. Chem. Phys.* **1969**, *51* (6), 2657−2664. (b) Collins, J. B.; von R. Schleyer, P.; Binkley, J. S.; Pople, J. A. Self-consistent molecular orbital methods. XVII. Geometries and binding energies of second-row molecules. A comparison of three basis sets. *J. Chem. Phys.* **1976**, *64* (12), 5142−5151.

(46) Dobbs, K. D.; Hehre, W. J. Molecular orbital theory of the properties of inorganic and organometallic compounds **5**. Extended basis sets for first-row transition metals. *J. Comput. Chem.* **1987**, *8* (6), 861−879.

(47) (a) Grimme, S.; Antony, J.; Ehrlich, S.; Krieg, H. A consistent and accurate ab initio parametrization of density functional dispersion correction (DFT-D) for the 94 elements H-Pu. *J. Chem. Phys.* **2010**, *132* (15), 154104. (b) Grimme, S.; Ehrlich, S.; Goerigk, L. Effect of the damping function in dispersion corrected density functional theory. *J. Comput. Chem.* **2011**, *32* (7), 1456−1465.

https://dx.doi.org/10.1021/acs.inorgchem.9b03097